Supplementary Information Text

Materials

L-AP4 (Cat. No. 0103), LY341495 (Cat. No. 1209/1), LY379268 (Cat. No. 2453) and L-Quisqualic acid (Cat. No. 0.188) were bought from Tocris Bioscience. Isopropyl β-D-1-thiogalactopyranoside (IPTG) (ref. I6758), L-glutamic acid hydrochloride (ref. G2128) and Poly-L-Ornithine (ref. P4957) were from Sigma-Aldrich. O^6-benzylcytosine (BC)-Lumi4-Tb (ref. SCLPTBF), BC-Green (ref. SCLPGRNF), O^6-benzylguanine (BG)-Lumi4Tb (ref. SSNPTBX), BG-Green (ref. SSNPGRNZ), anti-c-Myc-d2 (ref. 61MYCDAF) and Tag-lite® buffer (ref. LABMED) were kindly supplied by Cisbio Bioassays. BG-Cy3b was custom designed by Cisbio Bioassays. The plasmids encoding for the N-terminal SNAP-tag and CLIP-tag-labelled wild-type human and rat mGlu4 (1), rat mGlu2-C1KKXX (2) and rat SNAP-mGlu4-C2KKXX (3) have been described previously.

Methods

Llama immunization, selection, production and purification of DN45

The llama immunization, selection, production and purification of DN45 were performed as described previously (4). In brief, two llamas were immunized by four subcutaneous injections with 5×10^7 HEK293T cells, transfected with rat or human mGlu4 receptors. The V_HH library constructions were performed in *E. Coli* TG1 strains and the library diversity was above 10^9 transformants.

Bacteria were then infected by KM13 helper phage and phage-containing pellets were purified by two selection rounds on human mGlu4 receptor transfected in HEK293T (2×10^7) cells. Each round was preceded by a depletion step on cells that were not transfected and positive selections were performed in the presence of an excess of anti-HEK293 cells (5). *E. Coli* TG1 bacteria were infected with eluted phages and could be used for production of the nanobody.

The production of DN45 was done by transforming *E. Coli* BL21DE3 strain bacteria. They were grown overnight at 37 °C while agitating. Protein production was induced the day after by addition of 1 mM IPTG and bacteria were grown overnight at 28 °C while agitating. Bacteria were then collected and lysed in TES-buffer containing Tris, EDTA and sucrose. After centrifugation, the periplasmic extract was recovered and the His-tagged nanobodies were purified by Ni-NTA purification (Qiagen).

Mutagenesis

For the generation of rmG4-2M, rmG4-3M, rmG4-4MA, rmG4-4MB and rmG4-5M, synthethic genes encoding for the rat mGlu4 with corresponding mutations were ordered at GeneCust. The synthetic gene was inserted in a N-terminally SNAP-tagged rat mGlu4 receptor with the DNA ligation kit from Agilent Technologies. SNAP-rmG4-

5M-C2KKXX was generated by introducing the synthetic gene encoding for rmG4-5M into a N-terminally SNAP-tagged rat mGlu4 receptor with a C-terminal endoplasmic reticulum sequence C2KKXX. All other mutations were done by site-directed mutagenesis following the QuickChange mutagenesis protocol from Agilent Technologies.

Cell culture and transfection

HEK-293 (ATCC® CRL-1573™) cells were cultured in Dulbecco's Modified Eagle Medium (DMEM) (ref. 41965, Gibco™) containing 10% fetal bovine serum (FBS) (ref. F2442, Sigma-Aldrich). For each experiment we used 100,000 cells/well of a black 96-wells plate (ref. 655086, Greiner bio-one) coated with poly-L-ornithine (ref. P4957, Sigma-Aldrich). Cells were detached from the petridish (~80% confluency) with trypsin-EDTA (0.05%) (ref. 25300054, Gibco™) and after removal of the trypsin-EDTA by centrifuging, diluted in DMEM supplemented with 10% FBS.

Depending on the experiment, HEK-293 cells were transfected by electroporation (6) or reverse lipofectamine transfection following the manufacturer's protocol (Invitrogen™ Lipofectamine 2000™). To prevent toxic concentrations of glutamate in the medium, excitatory amino acid transporter 3 (EAAC1) was co-transfected. For binding experiments 9 µg of plasmid of the receptor and 1 µg EAAC1 were co-transfected by electroporation. For IP-1 accumulation experiments, 8 µg of plasmid of the receptor, 1 µg Gqi9 and 1 µg EAAC1 were co-transfected by electroporation. For the Gi-BRET assay, 4 µg of plasmid of the receptor, 0.8 µg Gi-Rluc, 0.8 µg Gβ, 1.6 µg Gγ-Venus and 1 µg EAAC1 were co-transfected by electroporation. For the mGlu2-4 biosensor experiment, 80 ng CLIP-mGlu2-C1KKXX, 40 ng SNAP-rmG4-5M-C2KKXX, 20 ng EAAC1 and 10 ng pRK6 empty vector per well were transfected by reverse

lipofectamine transfection. Cells were incubated for 24 hours at 37 °C and 5% CO_2 and medium was changed for pre-heated serum-free DMEM Glutamax (ref. 10566016, Gibco™) 2 hours before the start of the experiment.

Labelling of CLIP and SNAP-tag

Labelling of the CLIP and SNAP-tag with fluorescent molecules was done for 1 hour and 30 minutes at 37 °C in serum-free DMEM Glutamax. For expression and binding experiments for the mGlu4, the cells were incubated with 100 nM BG-Lumi4Tb. For measuring expression levels of the mGlu2-4, the cells were incubated with 1 µM BC-Lumi4Tb and 100 nM BG-Lumi4Tb. For binding on the mGlu2-4, the cells were incubated with 1 µM BC-Lumi4Tb. For the TR-FRET biosensor assay of the mGlu4, the cells were incubated with 100 nM BG-Lumi4Tb and 60 nM BG-Green. For the TR-FRET biosensor assay of the mGlu2-4, the cells were incubated with 100 nM BG-Lumi4Tb and 1 µM BC-Green. Unbound substrate was removed by washing each well four times with Tag-lite®-buffer.

DN45 binding and selectivity assay

Eight rat and eight human mGlu receptors were overexpressed in HEK293 cells as described in cell culture and transfection and incubated in a black 96-wells plate. Expression levels of the receptors were measured by the PHERAstar FS as the signal at 620 nm after excitation at 337 nm by a UV-pulsed nitrogen laser. Next, cells were pre-incubated for 30 minutes at 37 °C and 5% CO_2 with 10 µM L-AP4, 100 nM LY379268, 1 µM quisqualic acid or 100 µM LY341495 in Tag-lite®-buffer depending on the overexpressed receptor. Then,105 nM of DN45 and 200 nM anti-c-Myc-d2 were added at the same time and cells were incubated for 3 hours at 20 °C. As a negative

control, a nanobody against β-arrestin 2 containing the c-Myc sequence was added instead of DN45. TR-FRET was measured with the PHERAstar FS after excitation at 337 nm by a UV-pulsed nitrogen laser. Signals at 620 nm and 665 nm were integrated and the HTRF®-ratio was calculated as follows:

$$HTRF® - ratio = \frac{Signal\ 665\ nm}{Signal\ 620\ nm} \times\ 10{,}000$$

Values were normalized as the signal over the signal of the negative control.

IP-1 accumulation assay

Inositol phosphate (IP-1) accumulation was determined with the IP-One assay kit from Cisbio Bioassays (ref. 62IPAPEC). Cells had been prepared in a black 96-wells plate. Dilution ranges of DN45 and L-AP4 were prepared in stimulation buffer, added to the cells and incubated for 30 minutes at 37 °C and 5% CO_2. Then, cells were lysed by addition of IP1 labelled with d2 and anti-IP1 antibody labelled with Lumi4Tb in lysis buffer. The lysate was incubated for 1 hour at 20 °C and TR-FRET was measured with the PHERAstar FS and the HTRF®-ratio was determined. Values were normalized as the percentage of response to L-AP4.

mGlu2-4 and mGlu4 biosensor assay

Compounds were added to each well of a black 96-wells plate containing cells and incubated for 30 minutes at 37 °C and 5% CO_2 in Tag-lite®-buffer. In case of pre-incubation steps, compounds were pre-incubated 30 minutes at 37 °C and 5% CO_2 prior to addition of the other compounds. TR-FRET was measured with the PHERAstar FS after excitation at 337 nm by a UV-pulsed nitrogen laser. The signal at 520 nm was integrated and an acceptor ratio was calculated as described before (7):

$$Acceptor\ ratio\ (\mu s) = \frac{\int_{100}^{50} Signal\ at\ 520\ nm}{\int_{1600}^{1200} Signal\ at\ 520\ nm}$$

Values were normalized as the percentage of response to L-AP4.

BRET assay

Cells had been prepared in a black 96-wells plate. Coelenterazine and dilution ranges of DN45, L-AP4 were prepared in PBS buffer. The signals at 530 nm and 480 nm were measured by the Mithras LB 940 (Berthold). Coelenterazine was added and signals were measured for 10 minutes. Then, coelenterazine and compounds were added directly after each other. Signals were measured for 25 minutes and BRET-values were calculated by dividing the signals at 530 nm and 480 nm. Values were normalized as percentage of response to L-AP4.

Statistical analysis

Curve fitting and statistical analysis was done with Graphpad Prism software (version 9.0). Data are expressed as mean ± SEM of three or more individually performed experiments. The performed statistical analysis is explained in the corresponding figure legend. P-values<0.05 were considered significant.

Single-molecule FRET approach

Sample preparation and smFRET measurements

Sample preparation and smFRET measurements were done as previously described(8) with a few modifications as specified in the following.

Cell culture, transfection and membrane fraction preparation

HEK293T cells (ATCC CRL-3216, LGC Standards S.a.r.l., France) were grown in Gibco™ DMEM, high glucose, GlutaMAX™ Supplement, pyruvate (Thermo Fisher Scientific, France) supplemented with 10% (vol/vol) FBS (Sigma-Aldrich, France) at 37°C, 5% CO_2 in 25cm^2 flasks to approximately 80 % confluence. Transfection was carried out by mixing 4 µg SNAP-mGlu4 plasmid DNA and 8 µl Lipofectamine 2000 (Thermo Fisher Scientific, France) in 500 µl Gibco™ Opti-MEM™ I reduced serum medium (Thermo Fisher Scientific, France) and incubation at room temperature for 25 minutes. The mixture was then added to the cells in DMEM GlutaMax supplemented with10 % FBS and expression was carried out for 72h at 37°C and 5% CO_2. The medium was replaced once with fresh DMEM GlutaMax with 10 % FBS after 48h. SNAP-tag labeling was achieved by addition of 2 mL DMEM GlutaMax supplemented with 900 nM BG-Cy3b and 300 nM BG-d2 and carried out for 1.5 hours at 37°C and 5 % CO_2, followed by three washes with 5 mL PBS DPBS w/o Ca^{2+} and Mg^{2+} (Thermo Fischer Scientific, France) at ambient temperature. Then cells were detached mechanically using a cell scraper in DPBS and collected at 1000 x g and 22°C for 5 minutes. Cells were resuspended in cold hypotonic lysis buffer (10 mM HEPES pH 7.4, cOmplete™ protease inhibitor (Sigma-Aldrich, France)), frozen and stored at -80°C. For the preparation of membrane fractions cells were thawed on ice and passed 30-times through a 200 µL pipette tip. After two rounds of centrifugation at 500 x g and 4°C for 5 min, the supernatant was aliquoted and centrifuged at 21,000 x g and 4°C for 30 min to collect crude membranes. The pellets were washed once with 20 mM HEPES pH 7.4, 118 mM NaCl, flash frozen in liquid N_2 and stored at -80°C.

Detergent solubilization

Receptors were solubilized on ice by resuspension of crude membranes in acquisition buffer (20 mM Tris-HCl pH7.4, 118 mM NaCl, 1.2 mM KH_2PO_4, 1.2 mM $MgSO_4$, 4.7

mM KCl, 1.8 mM $CaCl_2$) supplemented with 1 % (w/v) lauryl maltose neopentyl glycol (LMNG, Anatrace purchased through CliniSciences, France) + 0.2 % (w/v) cholesteryl hemisuccinate tris salt (CHS Tris, Anatrace purchased through CliniSciences, France) for 5 min. Then Glyco-diosgenin (GDN, Avanti Polar Lipids purchased through Merck) was added (final detergent concentration 0.83 % LMNG + 0.167 % CHS Tris + 0.83 % GDN) and the solution was centrifuged for 10 min at 21,000 x g and 4°C. The supernatant was diluted 8.33-times in acquisition buffer and applied to a Zeba Spin Desalting Column (7 kDa cut-off, Thermo Fisher Scientific, France) equilibrated in acquisition buffer containing 0.005 % LMNG + 0.001 % CHS Tris + 0.005 % GDN and centrifuged 2 min at 1,500 x g and 4°C. The flow-through was then immediately diluted 10-times in cold acquisition buffer and kept on ice in the dark until use.

smFRET measurements

The pulsed interleaved excitation (PIE) – multiparameter fluorescence detection (MFD) setup, data acquisition and analysis were previously described.(8) Measurements were performed at a 4 times dilution of the sample in acquisition buffer without detergent and further dilution in acquisition buffer containing 0.0025 % LMNG, 0.0005 CHS tris, 0.0025 % GDN to achieve single molecule-compatible concentrations of labeled receptors (approximately 30-50 pM) in the absence of ligand or in presence of 100 µM LY34, 10 µM DN45 or 10 µM L-AP4. Apparent FRET efficiencies (E_{PR}) corrected for direct acceptor excitation and donor leakage into the acceptor channel were determined using the Software Package for Multiparameter Fluorescence Spectroscopy, Full Correlation and Multiparameter Fluorescence Imaging developed in C.A.M. Seidel's lab (http:// www.mpc.uni-duesseldorf.de/seidel/) as previously described.(9) FRET histograms were fitted using Origin 6 (Microcal Software, Inc.) and displayed in GraphPad Prism 7.05.

Molecular modelling

Homology model of mGlu4 VFT

The model for the mGlu4 homodimer was built using MODELER (10) as implemented in Discovery Studio. Two PDB structures 6BSZ (Human mGlu8 Receptor complexed with glutamate at 2.65 Å resolution) and 6BT5 (Human mGlu8 Receptor complexed with L-AP4 at 2.92 Å resolution) were used as templates. A disulfide bridge was defined between the Cys 136 of the two loops. The ligand L-AP4 from 6BT5 was used when constructing the model. We generated 100 models and the one with the lowest probability density factor (PDF) and lowest discrete optimized protein energy (DOPE) (11) score was selected.

Homology model of DN45

We then built the homology model of DN45 with the Model Antibody Cascade protocol from Discovery Studio 2020. This protocol automatically identified most similar PDB structures to model the framework and used 5GXB, 5IMM, 4LGS and 5M2W. The protocol also identifies the best templates for each CDR loop. For loop H1, it used loop H1 from PDB structures 5LMJ and EJ1. For loop H2, the templates were the H2 loop from 6EHG, 4TVS. Finally, for loop H3, the templates loops where from 5LWF and 1U0Q.

Docking of DN45 to mGlu4 VFT

The docking of DN45 to mGlu4 VFT was performed with ZDOCK (12) as implemented in Discovery Studio (BIOVIA, Dassault Systèmes, Discovery Studio Modeling Environment, Release 2020, San Diego: Dassault Systèmes, 2020). After generating 54000 poses, a filtering was then used to keep only poses where CDRs from the

nanobody DN45 were interacting with mGlu4. The distance criterion was 10 Å. The two first poses with the best ZRANK (13) score were in the same cluster, at the interface of the two lobes.

Refinement of Docked Structures

In order to refine the best pose generated with ZDOCK, we solvated the mGlu4 dimer-DN45 complex and the mGlu4 dimer-DN45-L-AP-4 complex in an orthorhombic periodic box of water with a minimum distance from boundary of 15.0 Å and performed with NAMD (14) a molecular dynamics simulation for 10 ns for each system. Analysis of trajectories and non-bonded interactions have been performed with Discovery Studio.

Virtual mutations

Using the last frame of the molecular dynamics simulation, we performed a virtual mutagenesis to identify residues in mGlu4 that are critical for binding to DN45. We used the Discovery Studio Calculate Mutation Energy Binding protocol (15) that evaluates the effect of mutations on the binding affinity of molecular partners in protein-protein and protein-ligand complexes. It performs combinatorial amino-acid scanning mutagenesis on a set of selected amino-acid residues by mutating them to one or more specified amino-acid types. The energy effect of each mutation on the binding affinity ($\Delta\Delta G_{mut}$) is calculated as the difference between the binding free energy ($\Delta\Delta G_{bind}$) in the mutated structure and wild type protein: $\Delta\Delta G_{mut} = \Delta\Delta G_{bind}$(mutant) - $\Delta\Delta G_{bind}$(wild type). The $\Delta\Delta G_{bind}$ is defined as the difference between the free energy of the complex and unbound state. All energy terms are calculated by CHARMm and the electrostatics energy is calculated using a Generalized Born implicit solvent model. The total energy

is calculated as an empirical weighted sum of van der Waals interactions (E_{vdW}), electrostatic interactions (ΔG_{elec}), an entropy contribution ($-TS_{sc}$) related to the changes in side-chain mobility, and a non-polar, surface dependent, contribution to solvation energy (ΔG_{np}).

This protocol was used to predict the impact of single or a combination of mutations of human residues to their rat counterpart. Finally, the full interaction surface between DN45 and human mGlu4 was scanned.

We also calculated the impact of a single point mutation of each of these interface residues to the overall stability of mGlu4 using the Calculate Mutation Energy Stability protocol (16). It performs combinatorial amino-acid scanning mutagenesis on a set of selected amino-acid residues by mutating each of them to one or more specified amino-acid types. The energy effect of each mutation on the protein stability (mutation energy, $\Delta\Delta G_{mut\text{-}stab}$) is calculated as the difference of the free energy of folding ($\Delta\Delta G_{folding}$) between the mutated structure and the wild type protein: $\Delta\Delta G_{mut\text{-}stab} = \Delta\Delta G_{folding}(\text{mutant}) - \Delta\Delta G_{folding}(\text{wild type})$. The $\Delta\Delta G_{folding}$ is defined as the free energy difference between the folded (ΔG_{fld}) and unfolded (denaturated) states (ΔG_{unf}) of the protein: $\Delta\Delta G_{folding} = \Delta G_{fld} - \Delta G_{unf}$. Note that a negative value of $\Delta\Delta G_{mut}$ indicates the mutation has a stabilizing effect, and conversely, a positive value indicates the mutation has a destabilizing effect. The energy of the folded state of the wild type is derived from the input structure. The structures of the mutants in the folded state are modeled by keeping the backbone rigid while optimizing the side-chains using the ChiRotor algorithm (17). Before evaluating the folding energy terms, the structures of the wild type and mutants are energy minimized using CHARMm. The unfolded state is modeled as a relaxed penta-peptide in an extended conformation with the mutated

residue in the center. The peptide model is applied only to the short range interactions involving the mutated residues and it is extended with a Gaussian chain model to account for the long-range electrostatic interactions. This is based on the hypothesis that most of the contacts between amino acid residues in the unfolded protein are only sporadic if the residues are not immediate neighbors along the sequence. Considering that van der Waals interactions decline sharply with distance and contribute only at very close contacts; the method neglects the non-polar interactions between the residues that are separated by more than two peptide bonds in sequence.

All energy terms are calculated by CHARMm, and the electrostatics energy is calculated using a Generalized Born implicit solvent model. The total energy is calculated as an empirical weighted sum of van der Waals (E_{vdW}) interaction, electrostatic interaction (ΔG_{elec}), an entropy contribution ($-TS_{sc}$) related to side-chain mobility, and a non-polar, surface dependent, contribution to solvation energy (ΔG_{np}). The calculations were performed in pH-dependent mode.

Supplementary Information References

1. P. Scholler, *et al.*, HTS-compatible FRET-based conformational sensors clarify membrane receptor activation. *Nat. Chem. Biol.* **13**, 372–380 (2017).
2. E. Doumazane, *et al.*, A new approach to analyze cell surface protein complexes reveals specific heterodimeric metabotropic glutamate receptors. *FASEB J.* **25**, 66–77 (2011).
3. J. Liu, *et al.*, Allosteric control of an asymmetric transduction in a G protein-coupled receptor heterodimer. *Elife* **6**, 1–19 (2017).
4. P. Scholler, *et al.*, Allosteric nanobodies uncover a role of hippocampal mGlu2 receptor homodimers in contextual fear consolidation. *Nat. Commun.* **8**, 1 (2017).
5. K. Even-Desrumeaux, *et al.*, Masked selection: A straightforward and flexible approach for the selection of binders against specific epitopes and differentially expressed proteins by phage display. *Mol. Cell. Proteomics* **13**, 653–665 (2014).
6. I. Brabet, M. Parmentier, C. De Colle, Comparative effect of L -CCG-I , DCG-IV and k -carboxy- L -glutamate on all cloned metabotropic glutamate receptor subtypes. *Neuropharmacology* **37**, 1043–1051 (1998).
7. P. Scholler, *et al.*, HTS-compatible FRET-based conformational sensors clarify membrane receptor activation. *Nat. Chem. Biol.* **13**, 372–380 (2017).
8. A. Cao, R. B. Quast, F. Fatemi, P. Rondard, Allosteric modulators enhance agonist efficacy by increasing the residence time of a GPCR in the active state. *Nat. Commun.* **in press** (2021).
9. L. Olofsson, *et al.*, Fine tuning of sub-millisecond conformational dynamics controls metabotropic glutamate receptors agonist efficacy. *Nat. Commun.* **5** (2014).
10. A. Sali, T. L. Blundell, Comparative Protein Modelling by Satisfaction of Spatial Restraints. *J. Mol. Biol.* **234**, 779–815 (1993).
11. M. Shen, A. Sali, Statistical potential for assessment and prediction of protein structures. *Protein Sci.* **15**, 2507–2524 (2006).
12. R. Chen, L. Li, Z. Weng, ZDOCK : An Initial-Stage Protein-Docking Algorithm. *PROTEIN Struct. Funct. Genet.* **52**, 80–87 (2003).
13. B. Pierce, Z. Weng, ZRANK: Reranking Protein Docking Predictions With an Optimized Energy Function. *PROTEIN Struct. Funct. Genet.* **67**, 1078–1086 (2007).
14. J. C. Phillips, *et al.*, Scalable Molecular Dynamics with NAMD. *J. Comput. Chem.* **26**, 1781–1802 (2005).
15. V. Z. Spassov, L. Yan, pH-Selective mutagenesis of protein–protein interfaces: In silico design of therapeutic antibodies with prolonged half-life. *PROTEINS Struct. Funct. Bioinforma.* **81**, 704–714 (2012).
16. V. Z. Spassov, L. Yan, A pH-dependent computational approach to the effect of mutations on protein stability. *J. Comput. Chem.* **37**, 2573–2587 (2016).
17. V. Z. Spassov, L. Yan, P. K. Flook, The dominant role of side-chain backbone interactions in structural realization of amino acid code. ChiRotor: A side-chain prediction algorithm based on side-chain backbone interactions. *Protein Sci.* **16**, 494–506 (2007).

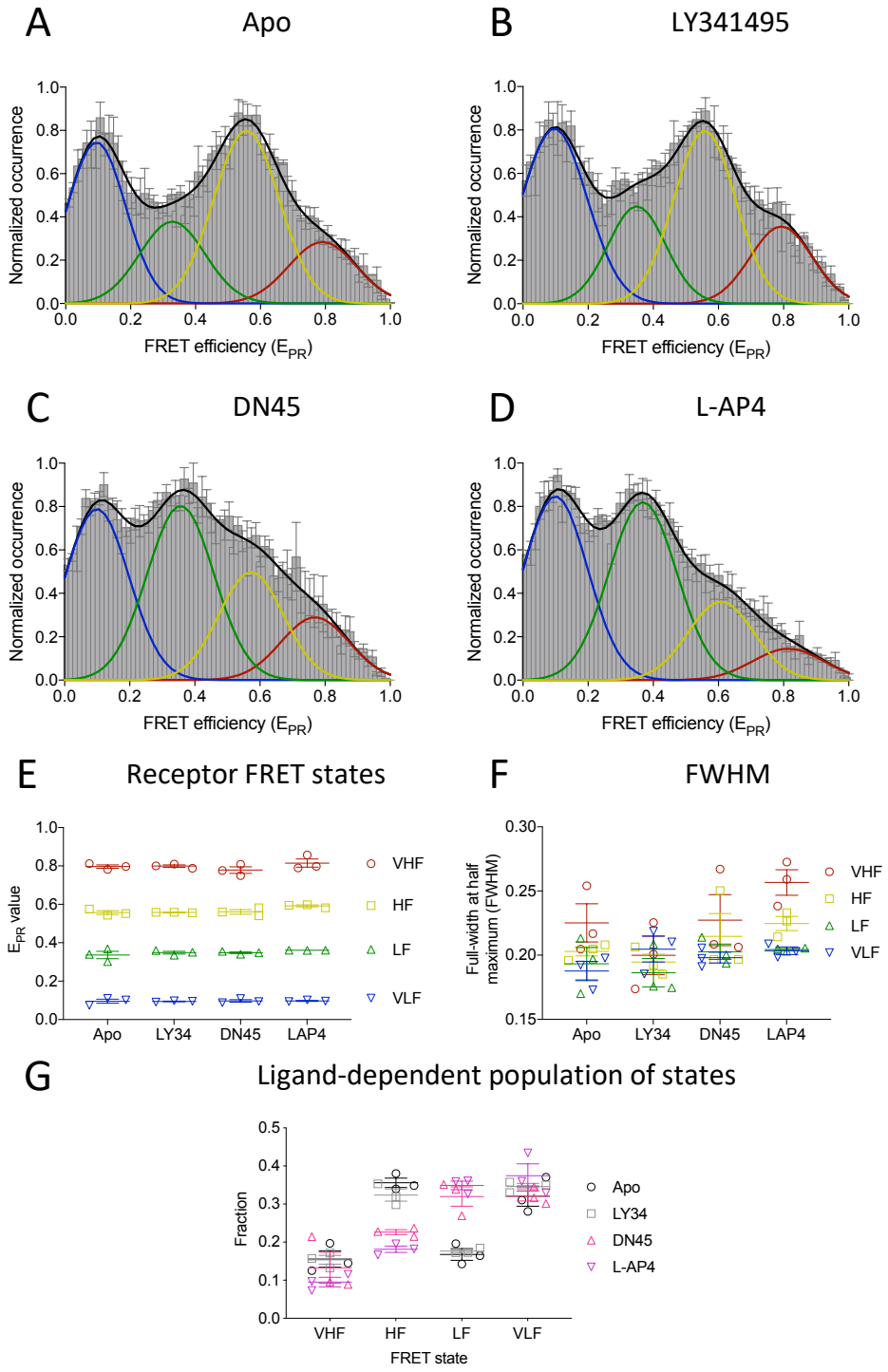

Fig. S1. Agonist action of DN45 nanobody on VFT reorientation analyzed by smFRET. *(A-D)* FRET efficiency histograms of mGlu4 dimers N-terminally SNAP-labeled with BG-Cy3b donor and BG-d2 acceptor fluorophores in the absence of ligand (Apo) or in the presence of DN45, LY341495 or L-AP4. The average global fit (black) as well as the very low FRET (VLF, blue), low FRET (LF, green), high FRET (HF,

yellow) and very high FRET (VHF, red) populations obtained by gaussian fitting using variable E_{PR} and full width half maximum (FWHM) values are shown. E) Mean E_{PR} and F) FWHM values for each of the four states under different ligand conditions. G) Fraction of each of the four states relative to all states under different ligand conditions. The histograms *A-D* show the mean number of molecules determined from three independent biological replicates each normalized to the maximum number per replicate with error bars given as SEM. Data of *E-G* are represented as mean ± SEM of three independent biological replicates.

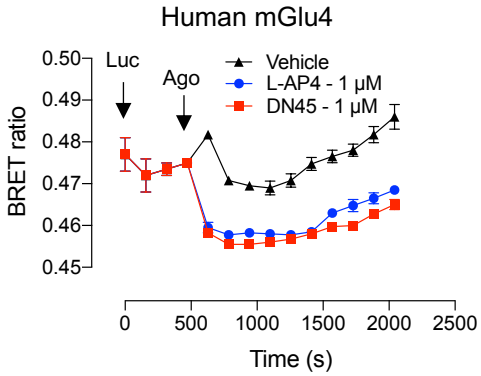

Fig. S2. Gi rearrangement kinetics visualized by change in BRET between Gαi-Rluc and Gγ-Venus. Signals were measured at 530 nm for the Venus and 480 nm for the Rluc. A basal signal was measured for 10 minutes after addition of coelenterazine (Luc). Next, the buffer and agonist conditions were added (Ago).

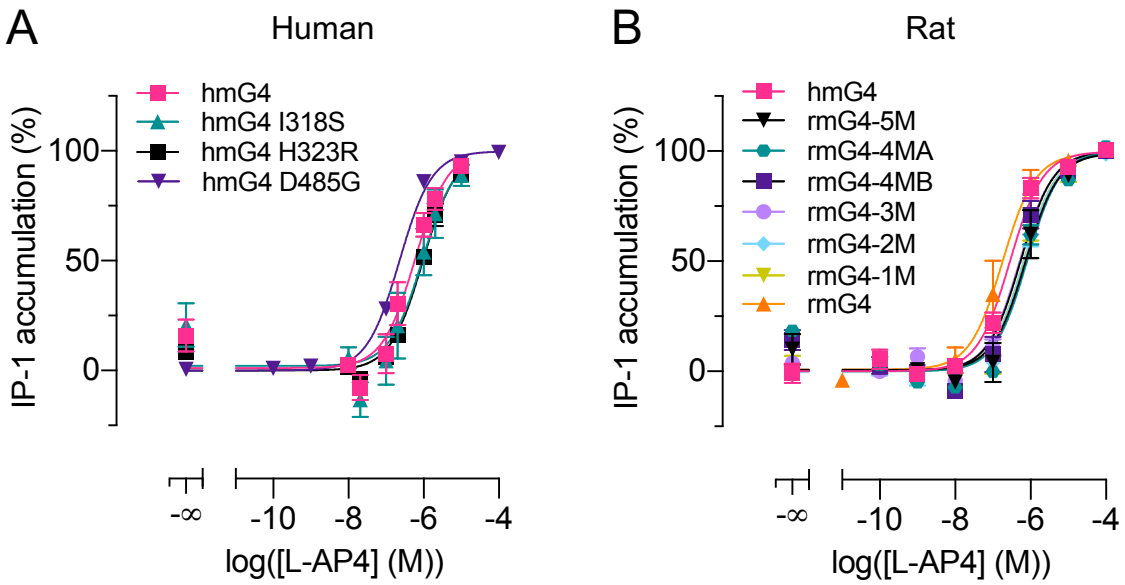

Fig. S3. Activation of human and rat mGlu4 constructs by L-AP4 in IP-1 accumulation assay. *(A)* IP-1 accumulation of human mGlu4 wild-type and mutated receptors. *(B)* IP-1 accumulation of the human and rat mGlu4 wild-type receptors and mutated rat mGlu4 receptors.

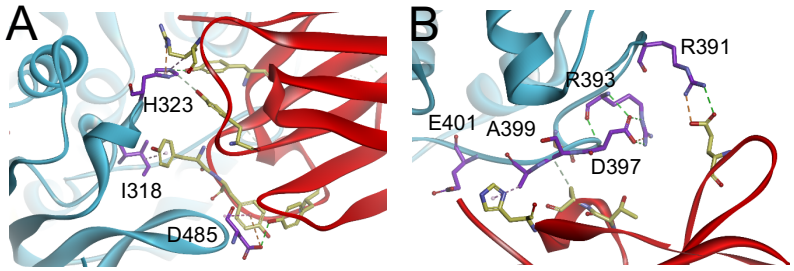

Fig. S4. Key interacting residues in the modelled complex of DN45 with human mGlu4 VFT (Fig. 3A). Residues of DN45 are displayed as yellow sticks, those of mGlu4 VFT in purple. *(A)* Lobe 2 and *(B)* lobe 1 interactions are shown as dashed lines (H-bonds are green, salt bridges are orange, hydrophobic interaction are purple).

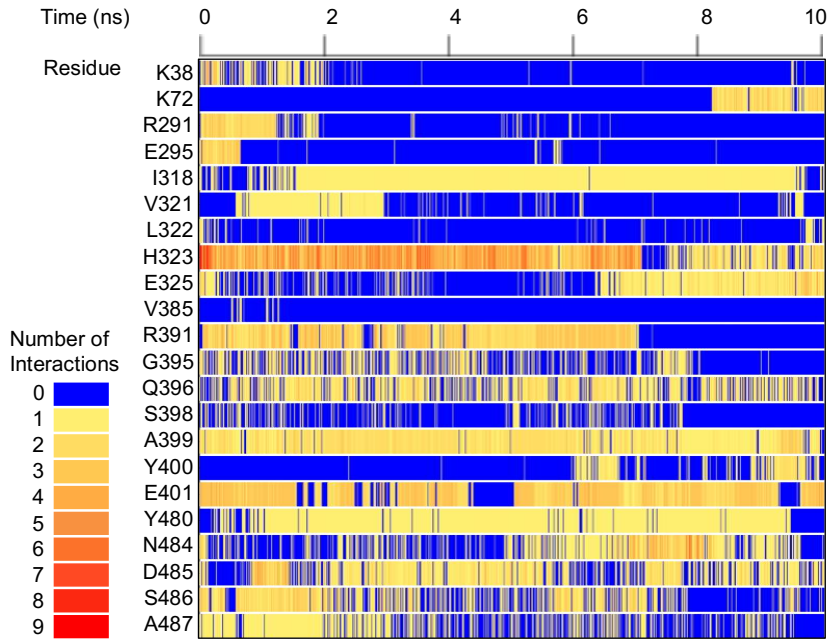

Fig. S5. Non-boned interactions as function of time for 10 ns molecular dynamics simulation of the docked DN45 mGlu4 complex for top interacting residues.

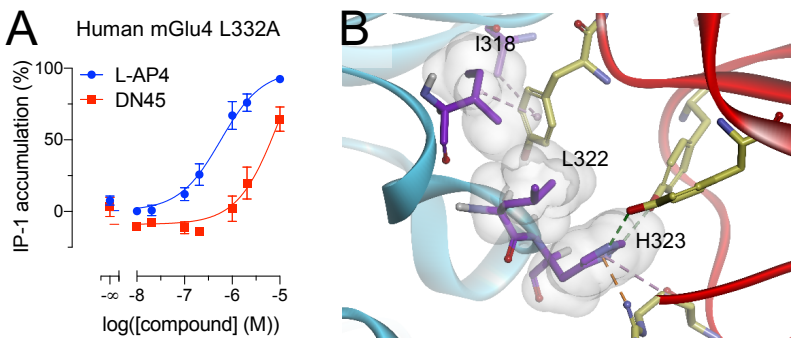

Fig. S6. Role of L322 in stabilizing interactions between the human mGlu4 VFT and DN45. *(A)* IP-1 accumulation induced by L-AP4 and DN45 on a human L322A mutated mGlu4 receptor. *(B)* Expanded view of Fig. 3A around residue L322 in the modelled complex of DN45 and the human mGlu4 VFT. Contacting residues in mGlu4 are displayed with light grey van der Waals surfaces.

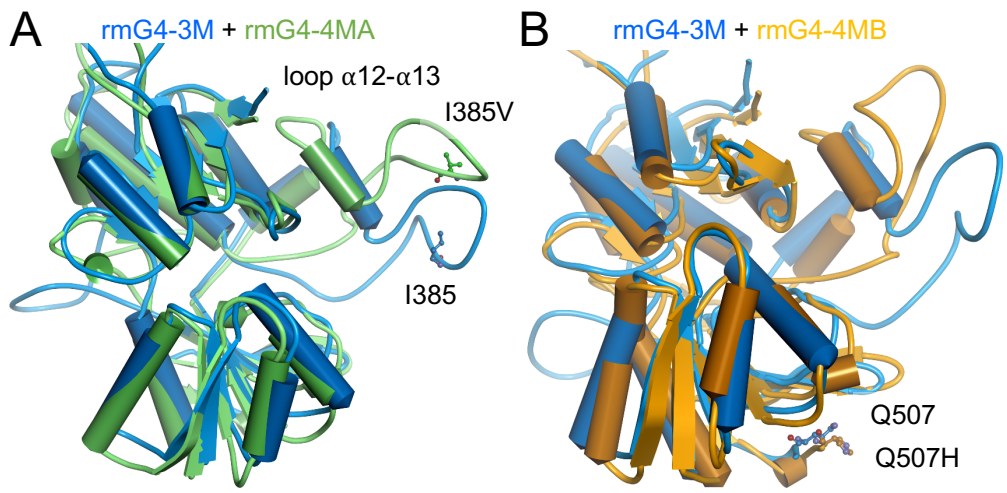

Fig. S7. Superimposition of VFTs of rmG4-3M and rmG4-4MA or rmG4-4MB models after 10 ns molecular dynamics simulation**.** *(A)* Superimposition of rmG4-3M and rmG4-4MA. *(B)* Superimposition of rmG4-3M and rmG4-4MB.

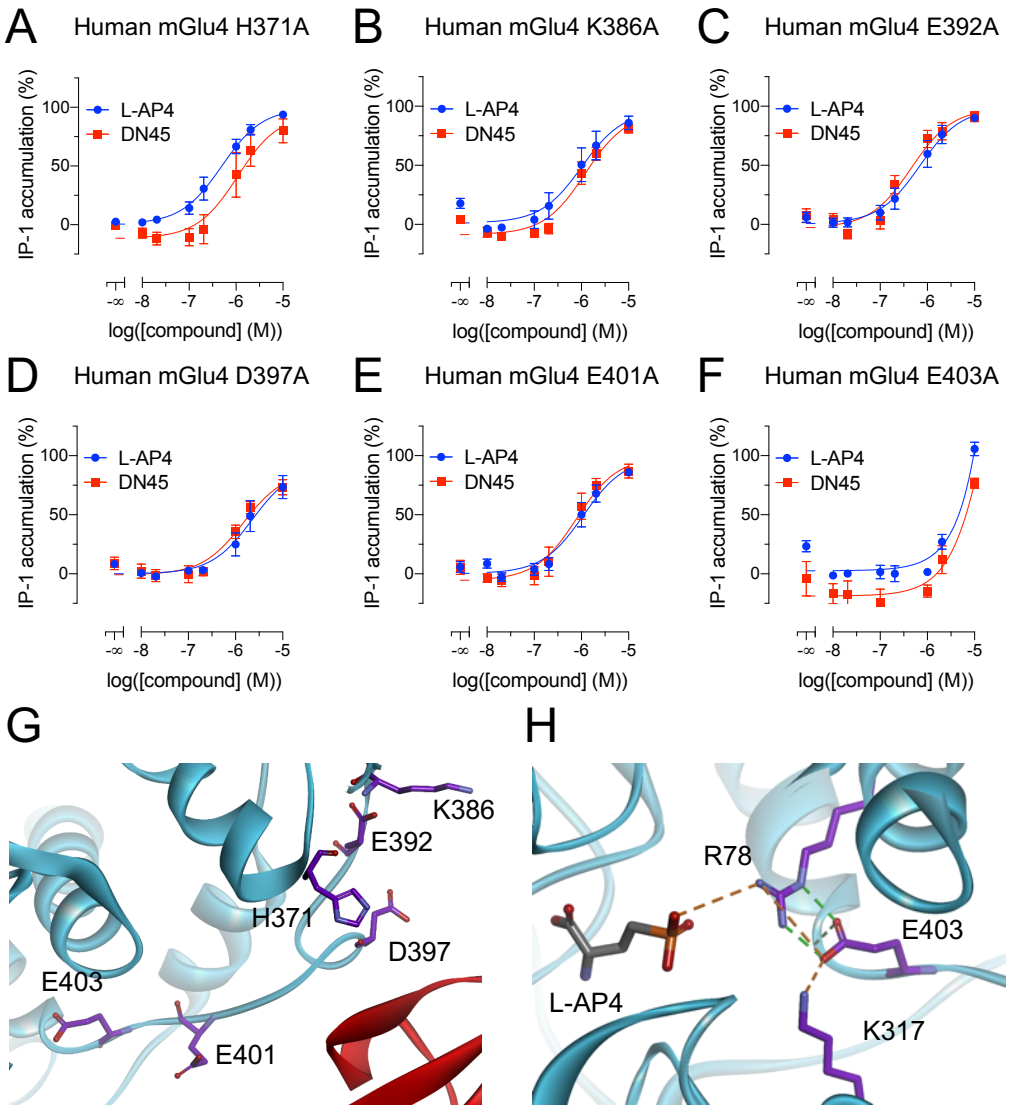

Fig. S8. Effect of alanine mutations on loop of lobe 1 of the human mGlu4 VFT. *(A-F)* Effect on the accumulation of IP-1 induced by L-AP4 and DN45 *(G-H)* 3D location of mutated residues in the modelled complex (Fig. 4). Note that E403 is stabilizing critical residues (R78 and K317) for L-AP4 binding explaining the decreased activation shown in panel F.

Table S1. Affinity (pK_D) and standard error of the mean (SEM) of DN45 for the different mGlu4 constructs. The used statistical analysis is mentioned in the main figure legends and values are compared with the control unless stated otherwise.

Fig.	Receptor	Condition	pKD ± SEM	N	P-value
1D	hmG4	+ 10 µM L-AP4	8.53 ± 0.09	3	-
3B	hmG4	+ 1 µM L-AP4	8.29 ± 0.02	3	Control
	hmG4 I318S	+ 1 µM L-AP4	8.00 ± 0.07	3	0.0168
	hmG4 H323R	+ 1 µM L-AP4	7.60 ± 0.06	3	0.0002
3D	hmG4	+ 1 µM L-AP4	8.28 ± 0.06	5	Control
	rmG4-5M	+ 1 µM L-AP4	7.70 ± 0.11	6	0.4613
	rmG4-4MA	+ 1 µM L-AP4	8.01 ± 0.10	3	0.9801
	rmG4-4MB	+ 1 µM L-AP4	7.93 ± 0.17	3	0.8392
5B	mGlu2-4	+ 10 µM L-AP4	8.34 ± 0.09	5	(L-AP4 vs Glu) = 0.1130
		+ 1 mM Glutamate	8.54 ± 0.10	5	(Glu vs LY37) = 0.0259
		+ 10 µM LY379268	8.14 ± 0.07	3	(LY37 vs L-AP4) = 0.4757

Table S2. Potency (pEC_{50}) and standard error of the mean (SEM) for the different mGlu4 constructs. The used statistical analysis is mentioned in the main figure legends and values are compared with the control.

Fig.	Receptor	Condition	pEC50 ± SEM	N	P-value
2A	hmG4	L-AP4	6.12 ± 0.03	3	Control
		DN45	6.57 ± 0.23	3	0.1222
2C	hmG4	L-AP4	7.22 ± 0.03	3	Control
		DN45	7.22 ± 0.11	3	0.9505
2D	hmG4	L-AP4	6.54 ± 0.10	3	Control
		DN45	6.65 ± 0.21	3	0.6674
		Glutamate	4.59 ± 0.15	3	-
2F	hmG4	L-AP4	6.16 ± 0.18	4	Control
		+ 5 nM DN45	5.96 ± 0.12	4	0.7166
		+ 10 nM DN45	6.19 ± 0.19	4	0.9990
		+ 100 nM DN45	5.74 ± 0.07	3	0.4949
3C	hmG4	DN45	6.63 ± 0.20	3	Control
	hmG4 I318S	DN45	5.68 ± 0.23	3	0.1794
	hmG4 H323R	DN45	5.07 ± 0.54	3	0.0367
3E	hmG4	DN45	6.65 ± 0.21	3	Control
	rmG4-5M	DN45	6.59 ± 0.54	3	0.7939
	rmG4-4MA	DN45	6.59 ± 0.02	3	0.9977
	rmG4-4MB	DN45	6.31 ± 0.08	3	0.7524
4C	hmG4 (A399N/E401S - N-Glycan)	L-AP4	6.05 ± 0.08	3	Control
	rmG4-4MA	DN45	5.18 ± 0.19	3	0.0070
4D	hmG4 (R391M+R393W+A399K)	L-AP4	5.74 ± 0.06	3	-
4E	hmG4 (H371E+R391M+R393W+A399K)	L-AP4	7.00 ± 0.01	3	-
		DN45	6.37 ± 0.06	3	-
4F	hmG4 (H371E+R391M+R393W+A399K)	L-AP4	6.85 ± 0.16	3	Control
		+ DN45	6.33 ± 0.13	3	0.0351
5C	mGlu2-4	+ LY37	6.11 ± 0.19	3	-
5D	mGlu2-4	LY37	6.02 ± 0.14	5	Control
		+ 10 µM DN45	8.49 ± 0.14	4	<0.0001

Table S3. Fraction and standard error of the mean (SEM) for single-molecule FRET analysis. The statistical analysis is mentioned in the main figure legend and values are compared to the control unless stated otherwise.

Fig.	Receptor	Condition	Fraction ± SEM	N	P-value
2B	hmG4	Apo	0.320 ± 0.025	3	Control
		LY34	0.353 ± 0.012	3	0.3263
		DN45	0.584 ± 0.014	3	<0.0001
		L-AP4	0.658 ± 0.005	3	<0.0001
		DN45 v. L-AP4			0.0073

Table S4. Impact on the binding of DN45 to hmGlu4 and overall stability of folding of the complex upon virtual mutation of twelve human residues to corresponding rat residues at the end of 10 ns simulation.

#	Human	Rat	Mutation energy binding (kcal/mol)	Effect	Mutation energy stability (kcal/mol)	Effect
66	P	A	0.07	Neutral	0.54	Destabilizing
224	V	L	-0.04	Neutral	1.22	Destabilizing
245	D	N	0.12	Neutral	0.53	Destabilizing
262	A	T	0.11	Neutral	-0.42	Neutral
270	R	K	0.02	Neutral	0.06	Neutral
280	A	G	0.09	Neutral	1.97	Destabilizing
281	V	I	0.01	Neutral	-0.06	Neutral
385	V	I	0.01	Neutral	-1.23	Stabilizing
507	H	Q	0.01	Neutral	-0.3	Neutral
318	I	S	1.55	Destabilizing	3.14	Destabilizing
323	H	R	2.96	Destabilizing	2.92	Destabilizing
485	D	G	0.69	Destabilizing	0.89	Destabilizing

Table S5. Predicted difference in binding energy of DN45 to rat mGlu4 upon mutation of 5 selected rat residues to corresponding human residues.

#	Rat	Human	Mutation energy binding (kcal/mol)	Effect
385	I	V	0.02	Neutral
507	Q	H	0.02	Neutral
318	S	I	-1.04	Stabilizing
323	R	H	-2.52	Stabilizing
485	G	D	-0.81	Stabilizing